TECHNISCHE MECHANIK, 30, 1-3, (2010), 269 – 279
submitted: October 31, 2009

Atomic-level structural change in Ni-Ti alloys under martensite and amorphous transformations

Ken-ichi Saitoh, Keisuke Kubota and Tomohiro Sato

The Ni-Ti alloys have been used widely as functional materials, especially for the purpose of superelastic behavior or shape memory effect. It has been believed that martensitic transformation (MT) between crystals plays a major role in the phase transition behavior, but recent experimental observation shows that there also exists stable amorphous structure. Detailed information of the atomic-level change, that is microscopic crystalline rearrangement of Ni-Ti alloys in applied shear deformation is needed. Our study aims at clarifying those atomic mechanisms by using molecular dynamics (MD) simulations. For Ni-Ti alloys, we assess the possibility of the modified version of EAM (MEAM) with parameters for Ni-Ti. We construct MD models to investigate both MT and amorphization in Ni-Ti alloys. We devise a method based on so-called common neighbor analysis (CNA) to effectively detects amorphous atoms, by finding clusters with five-folded symmetry (pentagonal bipyramids). In comparing models with different crystal orientation, when crystalline slip is not easy due to small resolved shear stress, the atoms in initial B2 or B19' structure tend to be rearranged with rotational motion and transform to amorphous atoms. Besides, there are "pre-amorphous" structures as a symptom of major and later increase of amorphous atoms.

1 Introduction

The Ni-Ti alloys are one of the most promising functional materials well used for engineering purpose. It is well known that they sometimes exhibit super-elastic behavior or shape memory effect, depending on sensitive choice of stoichiometry between Ni and Ti atoms (around 50:50) with a proper heat treatment. It is also understood that such behaviors in them are basically owing to martensitic transformation (MT). Atomistic and crystalline transition between austenite and martensite is important mechanism as well as microscopic twin formation or interaction. However, recently, the materials of this kind are explored experimentally as for amorphous phase formation (amorphization) especially in surface region. They are usually subjected to very strong shear deformation. These facts provide us the need of more thorough basic research on phase transition mechanisms furnished in Ni-Ti alloys. As atomic movement in MT behavior is displacive (diffusionless), no large displacement such as liquid-like diffusion occurs during the phase transition. Similarly, amorphization of metals or alloys can be carried out simply by slight movement of atoms within their crystal unit, from regular crystalline structure to non-regular (non-crystalline) one. However, in general, detailed mechanism of amorphization is still unclear in spite of extensive research activities.

Thus, this study focuses on atomic-scale and dynamic structural change of Ni-Ti alloy systems in MT and amorphization under applied external stress. Molecular dynamics (MD) simulation is supposed to be the most appropriate computational technique to acquire atomistic information since it is formulated to directly simulate dynamics of atoms. In MD, atoms are not bound to a prescribed crystal unit but they move only by means of interatomic interactions. Thus, it would be common understanding in MD study that choosing a potential function which is best fit to the observed system is crucial task. Therefore, we should try to construct an usable interatomic interaction and to compare the result with others. By doing

that, we could obtain fruitful perspective on atomic dynamics of Ni-Ti alloys.

As pointed out above, it has been extensively studied that shape-memory effect or super-elasticity in Ni-Ti alloys is based on MT mechanism. MD simulations on MT of Ni-Ti alloys have been discussed some times in literature (Sato et al. (2005), Suzuki and Shimono (2003), Ackland et al. (2008)). A crystal unit for austenite phase is called B2 cubic structure, while another unit for martensite is called B19' monoclinic structure. The B19' structure was once identified by experiment (Kudo et al. (1985), Otsuka and Ren (2005)). The validity of B19' structure, however, becomes controversial by a result of *ab initio* calculations conducted for crystalline unit (Ackland et al. (2008)). Of course, some interatomic potentials of embedded atom method (EAM) type have been developed (Farkas et al. (1996)), but to our knowledge there does not exist any potential function sufficient enough for Ni-Ti with martensite phase. The transition behavior between B2 and B19' structures is not so straightforward that it is difficult to clarify the behavior just by comparing energetic states of them. This is because we should consider the possibility of intermediate phases such as R phase, orthorhombic structure (bco), etc.

Recently, some observations of drawn wire or thin film of Ni-Ti alloys reveal that there are amorphous phases on the surface (Watanabe et al. (2002), Prokoshkin et al. (2005), Tsuchiya et al. (2009)). Microscopically, they can coexist with martensite or austenite phases. At this point, the potential function realizing amorphous structure of Ni-Ti system has not been obtained. But, this paper intends to show that a modified version of EAM (MEAM) potential for Ni-Ti system can be constructed and is effectively adopted to their amorphous structures. Besides, there is no theoretical framework of transition among three phases of Ni-Ti system, i.e. martensite, austenite, and amorphous. We will show the prediction that there is a certain relation between them. Our method is based on atom-by-atom detection of specific phases by means of so-called common neighbor analysis (CNA). The method is developed so as to find five-fold symmetry as for amorphous structure. Thus, by the results of MD simulation, atomistic view of transition between possible phases will be unveiled. Our present study emphasizes importance of atomistic (microscopic) understanding for MT or amorphization in Ni-Ti alloys. Of course, this would be accomplished with careful consideration as for interatomic potential and system size. It would be also done by extensive comparison with experimental facts. Anyway here, we show atomistic results and discuss on them.

This paper is organized as follows. First, we show set-up procedure of MD simulation including discussion on structure of Ni-Ti as well as potential function. Then, we show MD results of Ni-Ti specimens under shear deformation. In that, we discuss on inter-relation between amorphous phase and martensite/austenite phase. We show discovery concerning "pre-amorphous" atoms which are precursor of later amorphous formation. Finally we describe the conclusion of this study.

2 Theory and method

2.1 Interatomic potential for Ni-Ti

The crystal unit of Ni-Ti in austenite phase is B2 structure, the atoms on which is arranged in body-centered cubic (bcc) lattice. Because of high symmetry, B2 structure is easily realized by a simple potential function. On the other hand, B19' structure which is of martensite phase is hard to be realized by any simple framework of pairwise potential function, such as Lennard-Jones type (Suzuki and Shimono (2003)). Therefore, an EAM potential was constructed on experimental constant and values from *ab initio* calculation (Lai and Liu (2000)). The present authors have been utilizing the EAM potential and have reproduced the atomic behavior of Ni-Ti alloy. The points as for the EAM are summarized as follows (Sato et al. (2005), Sato et al. (2008)). (1)It is certain that the B19' monoclinic structure is certainly obtained as the most stable (minimized energy at 0 Kelvin). (2)Nevertheless, the minimum energy is very sensitive to the choice of cutoff length and crystal form. The energy of B2 unit lattice is

remarkably close to that of B19' unit lattice. (3)This EAM potential can be utilized to B2→B19' phase transformation, at least for stress-induced type.

In modeling amorphization, long range interaction is not preferable. Moreover, B19' is monoclinic lattice which has three unequal axes and one no-right angle. The tilted angle leads to dependence on atomic bonding angle. Considering these facts, in the present study, MEAM framework, a modified version of EAM (Baskes (1992)), is adopted. In the formulation of MEAM, atomic energy is given by,

$$\begin{aligned} E_i &= \left[F_i(\bar{\rho}_i/Z_i) + \frac{1}{2}\sum_{j(\neq i)} \phi(R_{ij}) \right] , \\ F(\bar{\rho}) &= AE_c \left(\frac{\bar{\rho}}{\bar{\rho^0}}\right) \ln\left(\frac{\bar{\rho}}{\bar{\rho^0}}\right) , \end{aligned} \tag{1}$$

where $F(\bar{\rho})$ is called embedded function and $\phi(R)$ is pairwise interaction. The electron density denoted by $\bar{\rho}$ and its reference value $\bar{\rho^0}$ are determined by somewhat complicated function including higher tensor terms in order to express the contribution of angular configuration. For example, the 1st order term of $\bar{\rho}$ for i atom is expressed as the sum of contribution from neighbor j atom,

$$(\rho_i^{(1)})^2 = \sum_\alpha \left\{ \sum_j \frac{R_{ij}^\alpha}{R_{ij}} \rho^{a(1)}(R_{ij}) \right\}^2 , \tag{2}$$

where variable with superscript α means a Cartesian component and $\rho^{a(1)}(r)$ is a simple pairwise function between i and j atoms.

Table 1 shows the parameters needed for the formulation of interactions in Ni and Ti system. The nomenclature of variables is exactly obeying one of literature (Kim et al. (2006)). Unfortunately, the parameters as for between Ni and Ti have not obtained yet. Therefore, we refer experimental data (Saitoh et al. (2006)) and include them in this table as our own new parameters. The cutoff length of interatomic interaction is 0.34 nm, which is in between the second and the third nearest neighbors of B2 structure.

Table 1: Parameters of MEAM potential function for Ni-Ti systems

Non-dimensional parameters for embedding function $F(\bar{\rho})$								
	A	$\beta^{(0)}$	$\beta^{(1)}$	$\beta^{(2)}$	$\beta^{(3)}$	$t(1)$	$t(2)$	$t(3)$
Ni	0.94	2.56	1.50	6.00	1.50	3.10	1.80	4.36
Ti	0.66	2.70	1.00	3.00	1.00	6.80	-2.00	-12.00

Parameters for Ni-Ni, Ti-Ti and Ni-Ti (our own) interactions)					
parameter	unit	Ni-Ni	Ti-Ti	Ni-Ti	(physical meaning)
E_c	eV	4.45	4.87	5.02	(cohesive energy)
r_e	nm	0.249	0.292	0.2607	(equilibrium distance)
B	10^{11} Pa	1.876	1.10	1.488	(bulk modulus)
D	-	0.05	0.00	0.025	(for Rose's universal function)

Besides, the higher tensor terms of electron density $\bar{\rho}$ in MEAM are quite in complication, especially when deriving interatomic force. In our opinion, by assessing and understanding error in the derivatives, the higher order terms in derivative of $\bar{\rho}$ could be omitted. On the other hand, energy formulation itself is effective and its calculation is carried out fully. Here we do not present the detailed expression for force, but it can be justified by consulting Table 2. It indicates that error (deviation of Hamiltonian) caused by omitting higher terms is small enough. Besides, in the actual MD simulation, more or less, those discrepancy can be discarded enough by temperature control technique.

Table 2: Energy drift caused by omitting higher force terms estimated in equilibrium (NVE) MD simulation for 8.0 ps (Ni-Ti in B2 structure composed of 1024 atoms.)

Initial temperature	10.0 K	300.0 K
Maximum drift in Hamiltonian (eV)	0.0381	0.0567

2.2 Detection method of martensite or amorphous

Since we usually define a crystal structure assuming full periodicity in collection of atomic positions, it seems hard to characterize each atom as a certain crystalline structure. However, by seeing local configuration within selected neighbor atoms, we are able to detect the centered atom as a specified crystalline structure. The one of famous methods is common neighbor analysis (CNA) (Honeycutt and Andersen (1987), Tsuzuki et al. (2007)). In CNA method, several local clustering structures are listed in advance and are compared with actual atomic configuration calculated by MD. The CNA method has succeeded in detecting fcc, hcp or bcc structure, together with lattice defects such as dislocation or stacking fault (Saitoh and Yonekawa (2010)). Usually, the result of CNA is presented by a series of four digits such as (1421),(1422), (1441), and (1661), etc. It will be shown that the CNA method can be applied to detect amorphous unit which may partially appear in crystals. It is also true that the existence of amorphous units is still controversial, but we define an unit structure as a cluster with five-folded symmetry (pentagonal bipyramid) theoretically proposed in literature (Farges et al. (1983)). The cluster comes to correspond to the CNA digits of (1551) as shown in Fig.1. Accordingly, if we obtain (1551) digits from snapshot of MD simulation, the centered atom is to be detected as "amorphous".

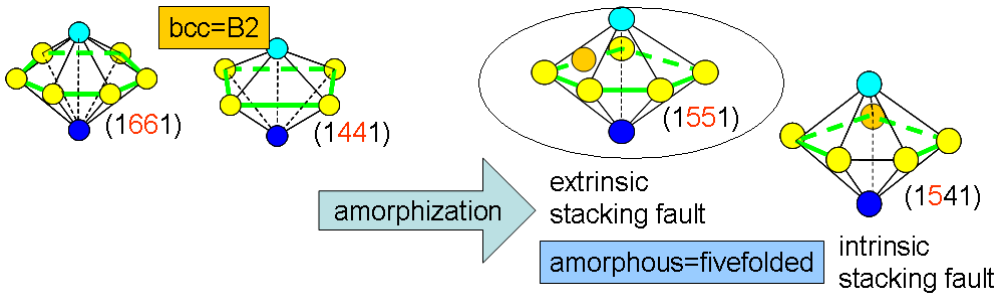

Figure 1: Concept and definition of amorphous unit by using CNA methods

On the other hand, martensite structure is bound to crystalline system. So, it is detected by comparing axes or angle inside the crystal unit with those of reference B19' structure. The reference lengths and angles for B19' unit may have relatively wide range as pointed out before (Saitoh et al. (2006)). Therefore, ranges for detection are set on lengths a and b, the ration b/a, and angle γ between a and b. If any triplet of neighbor atoms falls within those ranges, those atoms are to be detected as martensite (Saitoh et al. (2006)). The ranges for detection are:

- 0.279 nm$\leq a \leq$0.296 nm, 0.450 nm$\leq b \leq$0.476 nm, $1.51 \leq b/a \leq$1.66
- 96.3 deg.$\leq \gamma \leq$ 98.6 deg.

In particular, bonding angle γ is adjusted so as to take into consideration of several experimental values.

2.3 MD computation: models and conditions

Since experimentally amorphization is observed in heavy shear deformation, the MD specimen is also applied large simple shear. The outline of MD models is depicted in Fig.2.

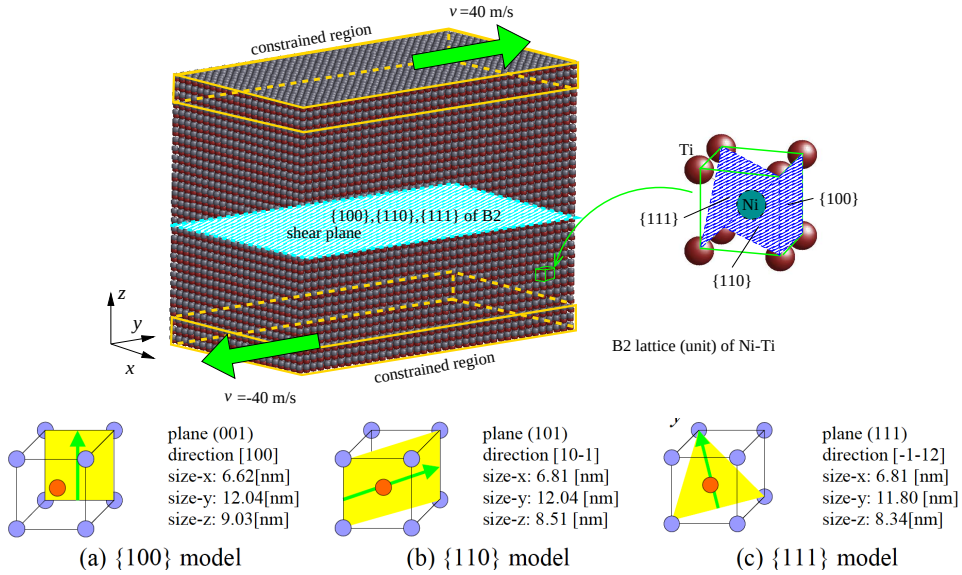

Figure 2: Molecular dynamics model for shear deformation of Ni-Ti system

First, a perfect crystal in B2 structure is fully equilibrated in 80.0 Kelvin and the stable structure is obtained. Then, by chucking two regions located on the top and the bottom, simple shear strain γ_{zy} is applied. Periodic condition is imposed on x and y directions. The present strain rate of the order of 10^9 1/s is computationally natural but remarkably high in experiment. We can believe that actual atoms tend to move in the same way as our computation, except for diffusive behavior. Of course, we should not omit the importance of strain rate, but we do not discuss it here.

MT or amorphization is closely related to crystalline orientation with regard to shearing direction and plane. Therefore, we construct three models with different orientations. They are named $\{100\}$, $\{110\}$ and $\{111\}$ models, as shown in Fig.2, which have $\{100\}$, $\{110\}$ and $\{111\}$ planes of B2 lattice as shearing plane, respectively. All models have almost the same dimensions and are also periodic in x and y directions. Incidentally, the slip system of B2 structure is $\{110\}\langle 111\rangle$ does not completely correspond to shear direction (y) of any model. As regards to the same γ_{zy}, the resolved shear stress (RSS) on each stacking plane is estimated in the order: $RSS_{\{110\}} > RSS_{\{100\}} > RSS_{\{111\}}$. Other calculation conditions are summarized in Table 3.

Table 3: Calculation condition for MD simulations

	unit	properties		
		$\{100\}$ model	$\{110\}$ model	$\{111\}$ model
The number of atom	—	52800	51200	49152
Strain rate	$10^9$1/s	8.86	9.40	9.59
The number of constrained atoms	—	7040	5120	4096
cell size (in x)	nm	6.622	6.811	6.811
cell size (in y)	nm	12.040	12.040	11.797
cell size (in z)	nm	9.030	8.514	8.342
System temperature (controlled)	K	80.0	80.0	80.0

3 Results and discussions

3.1 Transition behavior of martensite and amorphous structures

Figure 3 shows atomic configuration for model $\{100\}$, in which amorphization or martensite transformation occurs by shear loading. In the figures, drawing of atoms with initial B2 cubic structure are omitted in order that others are recognized easily. First, as shown in Fig.3(a), martensite (M) phase starts as nucleation in center region. The fact that the nucleation site avoids any region with strong constraint means that martensitic transformation is induced by averaged shear stress. Then, as shown in Fig.3(b), amorphous (A) phase appears near the bottom region where the M phase has already appeared. This signifies that the A phase is built as a subsequent structure of the M phase. After then, as shown in Fig.3(c), the A phase spreads all over the computation box. The A phase spatially distributes in combination with M phase. As a results, there are atoms which are detected as both M and A phases.

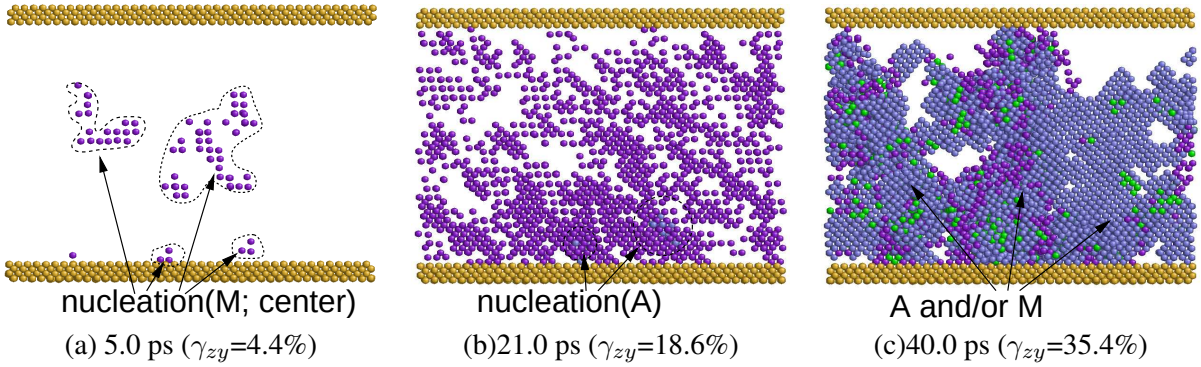

(a) 5.0 ps (γ_{zy}=4.4%) (b)21.0 ps (γ_{zy}=18.6%) (c)40.0 ps (γ_{zy}=35.4%)

Figure 3: Visualization of martensite (M) and amorphous (A) phases during shear deformation: the case of $\{100\}$ model

As predicted, models with three different orientation show the variety of nucleation and the way of phase transformation. Fig.4 are comparing $\{100\}$,$\{110\}$ and $\{111\}$ models at almost the same shear strain (γ_{zy} $\approx$0.25). As explained above, in the $\{100\}$ model, nucleation of A or M phase occurs at random position and the resulted phase becomes complicated. On the other hand, in $\{110\}$ model, M or A phase just appears near top and bottom regions. Some atoms near center region may be possibly once detected as M or A phase in a very short duration, but most of them finally returns to initial B2 structure. Slip plane common to B2 (austenite) and B19' (martensite) crystals is $\{110\}$. Therefore, $\{110\}$ model has well compatibility between slip plane and shear direction. In this case, slips between stacking planes occur in the center and phase transition is apt not to take place. The elastic energy stored by shear can be released just by those slips. The top and bottom regions are always distorted due to constraint. As slip is restricted there, A or M atoms can remain there.

The $\{111\}$ model shows a kind of "lamella" structure of new phases. In this case, the A phase and the M phase are connecting with each other in the same "lamella". The stretching direction of these "lamella" is not necessarily correspond to intrinsic slip systems, $\{110\}\langle 111\rangle$.

3.2 Relation between martensite and amorphous structures

In order to quantify the amount of amorphous (A) or martensite (M) phases (atoms), we checked time transition of each ratio. The ratio means the fraction of atoms detected as A or M phase to all the atoms in the system. The results are shown in Fig.5. As shown in these figures, shear strain at a burst of the A phase does not match to that of the M phase. The occurrence of the A phase generally follows M phase. Typically in $\{100\}$ model, at first the M atoms raises up to 13% at strain of 0.20, secondly the A atoms

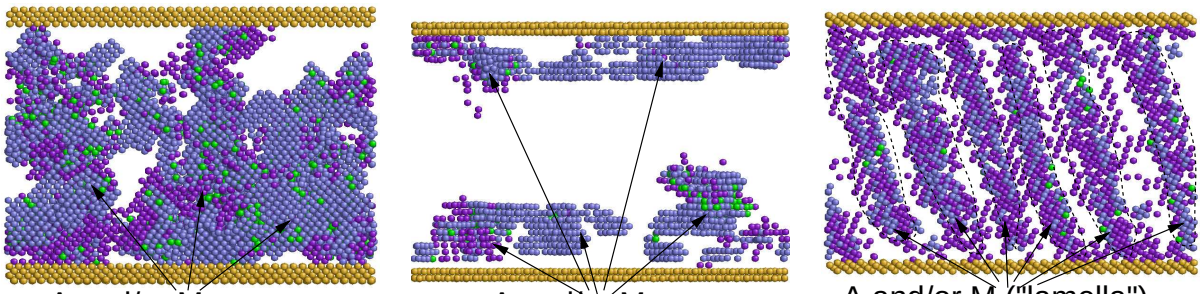

(a){100} model (γ_{zy}=24.8%) (b){110} model (γ_{zy}=26.3%) (c){111} model (γ_{zy}=26.8%)

Figure 4: Visualization of nucleation of martensite and amorphous phases : comparison of three models

increases at strain of 0.24. Reduction of B2 atoms corresponds to the increase of M phase. Finally, the B2 atoms recovers up to 70% in {100} model, when the increase of A phase is already saturated. By these observations, a mechanism is schematically suggested as shown in Fig.6. The atoms in B2 cubic crystal changes first to the M phase, then some of them changes secondly to the A phase, after that the transformed atoms (A or M) partly return back to B2 austenite finally.

Here again, we should note that the difference between three models. Quite unique behavior is found in {111} model. As shown in Fig.5(c), increase of the A atoms (burst of amorphization) is two-folded. The A atoms once increase up to 7% (the first increase) after the burst of M atoms, but then they diminish for a moment and again it almost doubles (the second increase). The first increase is likely to be a symptom of full transformation. Thus the atoms showing such behavior could be called "pre-amorphous (p-A)". It is assured by Fig.5(c) or observation of visualized movie that such short-lived "pre-amorphous (p-A)" atoms exist.

The resistance to shear deformation can be deduced from shear stress and shear strain curve (S-S curve). The comparison for three models are shown in Fig.7. In any case, yield occurs. The level of yield stress is the smallest in {111} model. Besides, yield strains are found at 19%, 19%, 28% for {100},{110}, {111} models, respectively (denoted by yield{hkl} in Fig.7). The yield point of {100} or {110} model corresponds to maximum ratio of the M atoms (denoted by M{100} or M{110} in Fig.7), whereas that for {111} model corresponds to the pre- or the major increase of A atoms (denoted by p-A{111} or A{111} in Fig.7). This fact substantiates that the configuration of {111} model possesses an unique mechanism of transformation. The mechanism is investigated more from atomistic viewpoint in the next part.

3.3 Behavior of phase transition in atomistic resolution

It is insightful to see the detailed behavior of atomic groups which are arbitrarily selected from the present Ni-Ti specimens. Those atoms are initially located in a confined region not so close to velocity-constrained regions at top and bottom. In Fig.8, the atomic motions in {110} and {111} models are compared, by viewing from a direction perpendicular to each shear plane, i.e. ⟨110⟩ for {110} model or ⟨111⟩ for {111} model. In {110} model, it is obvious that slip does occur parallel to viewing plane and the initial projected area has been stretched in y direction. On the other hand, in {111} model, the atoms try to move with rotational motion to fit their crystalline orientation to slip system. In this case, slip is remarkably suppressed due to small $RSS_{\{111\}}$. Accordingly, atoms have to rotate diffusively inside small region. In the meantime they lost crystalline structure and transform into amorphous structure. As shown in Fig.5, the {111} model produces more A atoms (nearly 30%) than other two models. It is concluded that, if slip motion is controlled for a low amount, amorphization can be enhanced by shear deformation.

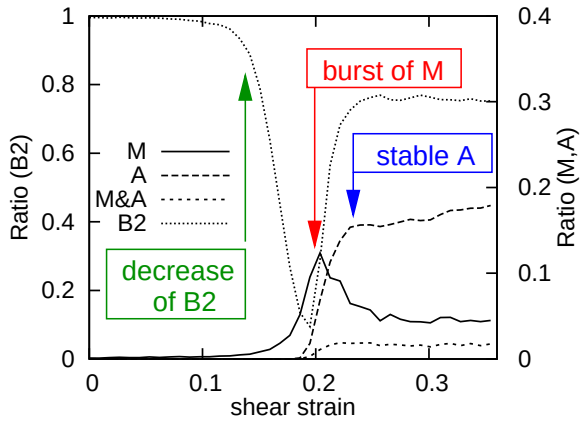

(a){100} model

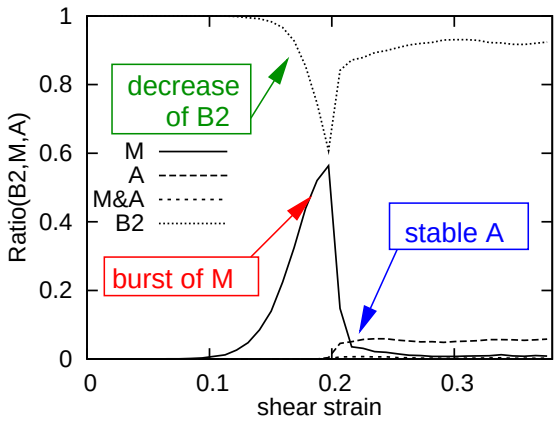

(b){110} model

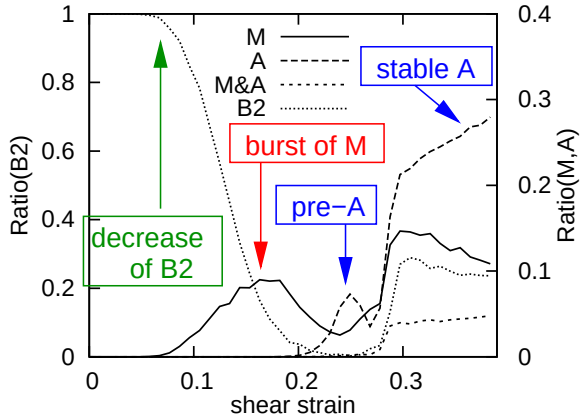

(c){111} model

Figure 5: Time transition of atomic ratio: martensite(M) / amorphous(A) / common(both M and A) / B2(initial) atoms (note that each is referring to one of two vertical axes.)

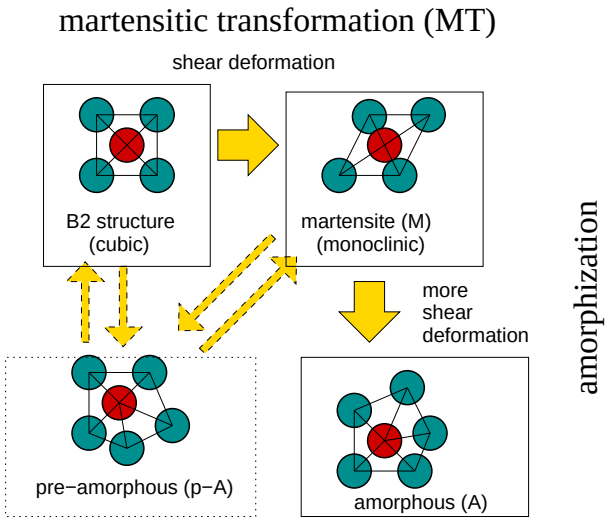

Figure 6: The supposed mechanism of phase transformation in Ni-Ti including amorphization: the schematic

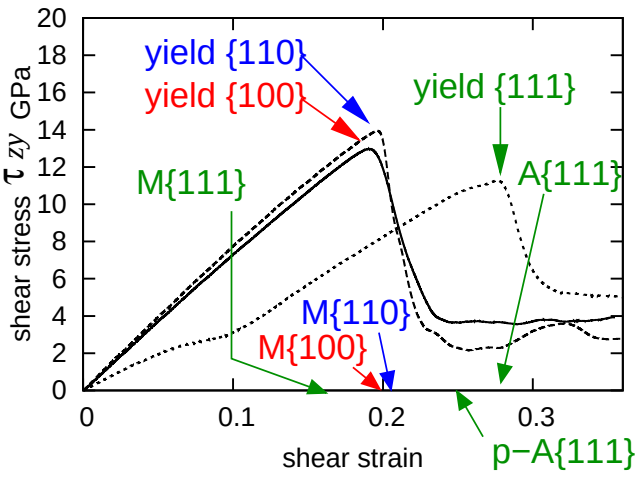

Figure 7: Shear stress and shear strain relation for three models

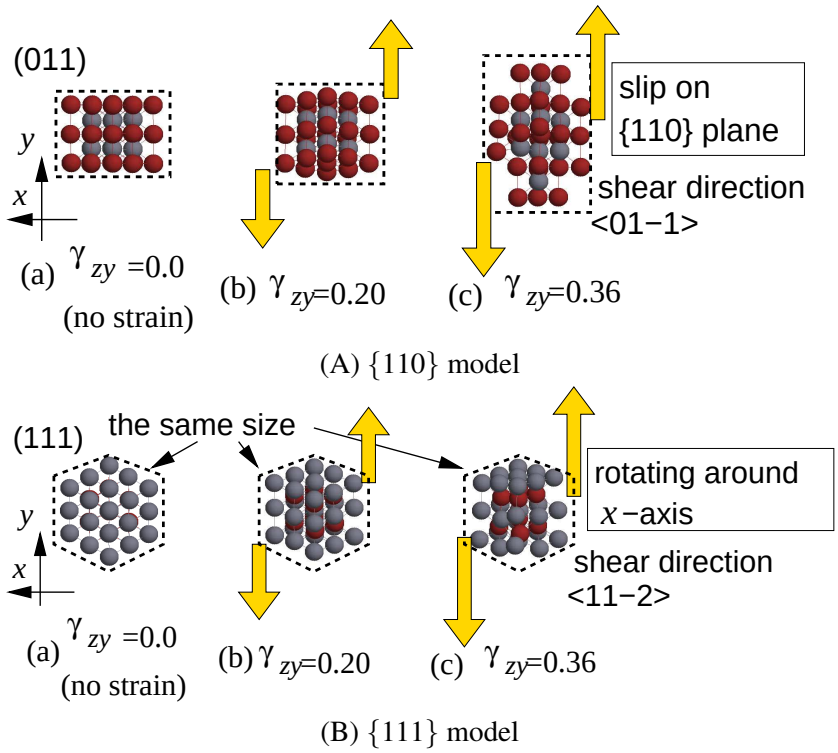

Figure 8: Detailed visualization of atomic configurations during shear loading: viewing direction is $\langle 110 \rangle$ for $\{110\}$ model and $\langle 111 \rangle$ for $\{111\}$ model(i.e. perpendicular to shear plane). Dark gray (red) atoms show titanium and light gray (gray) ones do nickel.)

The way from cubic crystal(B2) or martensite(M) phase into amorphous (A) phase is understood based on CNA method. In our CNA method, A atoms are characterized by CNA digits (1551). The neighboring atoms form a cluster denoted by (1551) as shown in Fig.1. The (1551) cluster can be produced from a previous crystalline cluster denoted by (1441) or (1661). Since (1661) is basically composed of six-atomic ring, one of them escapes from the cluster and remaining 5 neighbors become the (1551) cluster. Conversely, the (1441) cluster which is built by four atomic ring accepts new atom from external region, then the (1551) cluster is made. In either way, the resulted amorphous cluster with five-folded symmetry can be produced from the previous cluster of crystalline phase with small displacement of atoms.

4 Conclusion

Martensitic transformation (MT) or amorphization taking place in Ni-Ti alloy is investigated by means of molecular dynamics simulation (MD). The results are summarized as follows.

1. A modified version of EAM (MEAM) potential function is adjusted for Ni-Ti system with some approximation. The potential function can be applied to simulation of amorphization as well as simulation of MT.
2. The CNA method can be applied to detect amorphous atoms by specifying a CNA cluster with five-fold symmetry.
3. Transformation into amorphous phase occurs after martensite phase is obtained. When shear plane is parallel to $\{111\}$, there emerge "pre-amorphous" atoms which are the symptom of substantial amorphous atoms later.
4. When crystalline slip is suppressed, positions of atoms are reconfigured with rotational motion. By this mechanism, amorphization could be enhanced by restricting slip in shear deformation.

Acknowledgements

This work was supported by JSPS KAKENHI(21560103) (2009) and HRC Kansai university.

References

Ackland, G.; Jones, A.; Noble-Eddy, R.: Molecular dynamics simulations of the martensitic phase transition process. *Mater.Sci.Eng.,A*, 481-482, (2008), 11 – 17.

Baskes, M.: Modified embedded-atom poitential for cubic materials and impurities. *Phys.Rev.,B*, 46, 5, (1992), 2727 – 2742.

Farges, J.; de Feraudy, M.; Raoult, B.; Torchet, G.: Noncrystalline structure of argon cluster. i. polyicosahedral structure of ar$_n$ clusters, $20 < n < 50$. *J.Chem.Phys.*, 78, (1983), 5067 – 5080.

Farkas, D.; Roqueta, D.; Vilette, A.; Ternesx, K.: Atomistic simulations in ternary ni-ti-al alloys. *Model.Simul.Mater.Sci.Eng.*, 4, (1996), 359 – 369.

Honeycutt, J.; Andersen, H.: Molecular dynamics study of melting and freezing of small lennard-jones clusters. *J.Phys.Chem.*, 19, (1987), 4950 – 4963.

Kim, Y.-M.; Lee, B.-J.; Baskes, M.: Modified embedded-atom method interatomic potentials for ti and zr. *Phys.Rev.,B*, 74, (2006), 014101,1 – 12.

Kudo, Y.; Tokonami, M.; Miyazaki, S.; Otsuka, K.: Crystal structure of the martensite in ti-49.2 at.%ni alloy analyzed by the single crystal x-ray diffraction method. *Acta Metall.*, 33, 11, (1985), 2049 – 2056.

Lai, W.; Liu, B.: Lattice stability of some ni-ti alloy phases versus their chemical composition and disordering. *J.Phys.Condens.Mater.*, 12, (2000), L53 – L60.

Otsuka, K.; Ren, X.: Physical metallurgy of tini-based shape memory alloys. *Progress in Mater.Sci.*, 50, (2005), 511 – 678.

Prokoshkin, S.; Khmelevskaya, I.; Dobatkin, S.; Trubitsyna, I.; Tatyanin, E.; Stolyarov, V.; Prokofiev, E.: Alloy composition, deformation temperature, pressure and post-deformation annealing effects in severely deformed ti-ni based shape memory alloys. *Acta Mater.*, 53, (2005), 2703 – 2714.

Saitoh, K.; Sato, T.; Shinke, N.: Atomic dynamics and energetics of martensitic transformation in nickel-titanium shape memory alloy. *Materals Transactions*, 47, 3, (2006), 742 – 749.

Saitoh, K.; Yonekawa, Y.: Molecular dynamics study of extraordinary elastic deformation found in gold atomic cluster. *Journal of Advanced Mechanical Design, Systems, and Manufacturing*, 3, (2010), in press.

Sato, T.; Saitoh, K.; Shike, N.: Molecular dynamics study on microscopic mechanism for phase transformation of ni-ti alloy. *Model.Simul.Mater.Sci.Eng.*, 14, 5, (2005), S39 – S46.

Sato, T.; Saitoh, K.; Shike, N.: Atomistic modelling of ni-ti alloy on reversible phase transformations: a molecular dynamics study. *Mater.Sci.Eng.,A*, 481-482, (2008), 250 – 253.

Suzuki, T.; Shimono, M.: A simple model for martensitic transformation. *J. Phys. IV France*, 112, (2003), 129.

Tsuchiya, K.; Hada, Y.; Koyano, T.; Nakajima, K.; Ohnuma, M.; Koike, T.; Y., T.; Umemoto, M.: Production of tini amorphous/nanocrystalline wires with high strength and elastic modulus by severe cold drawing. *Scripta Materiallia*, 60, (2009), 749 – 752.

Tsuzuki, H.; Branicio, P.; Rino.J.P.: Structural characterization of deformed crystals by analysis of common atomic neighborhood. *Comput.Phys.Commun.*, 177, (2007), 518 – 523.

Watanabe, S.; Haishi, Y.; Suda, T.; Ohnuki, S.; Takahashi, H.; Kiritani, M.: Atomic analysis of stress-induced local amorphization in niti alloy. *Radiation Effects and Defects in Solids*, 157, (2002), 101 – 108.

Addresses: Ken-ichi Saitoh, Department of Mechanical Engineering, Kansai University 3-3-35 Yamatecho, Suita, Osaka, 564-8680 Japan
email: saitou@kansai-u.ac.jp
Keisuke Kubota, Komatsu Ltd,, Japan
Tomohiro Sato, Institute of Nano Technology, Kurimoto Ltd.